Modern Physics Letters A

IMPLEMENTATION OF THE ATLAS-SUSY-2018-04 ANALYSIS IN THE MADANALYSIS 5 FRAMEWORK

JONGWON LIM
Department of Physics, Hanyang University, Seoul 04763, Republic of Korea

CHIH-TING LU
School of Physics, KIAS, Seoul 02455, Republic of Korea

JAE-HYEON PARK
School of Physics, KIAS, Seoul 02455, Republic of Korea

JIWON PARK
Department of Physics, Hanyang University, Seoul 04763, Republic of Korea

We present the MadAnalysis 5 implementation and validation of the ATLAS-SUSY-2018-04 search. This ATLAS analysis targets direct stau production in events with two hadronic tau leptons, and probes 139 fb^{-1} of LHC proton-proton collisions at a center-of-mass energy of 13 TeV. The validation of our re-implementation relies on a comparison of our cutflow predictions with the auxiliary material and official results provided by the ATLAS collaboration in the context of two supersymmetry-inspired simplified benchmark models in which the Standard Model is extended by a neutralino and a stau decaying into a tau lepton and a neutralino. A first scenario focuses on very light staus, whereas a second one addresses heavier staus. Our predictions have been found to agree with ATLAS official cutflows at the level of 6%–8% in the heavy stau scenario, and exhibit a larger discrepancy (of 15%–50%) in the light stau scenario. This disagreement is however considered as not too significant, as both ATLAS and MadAnalysis 5 predictions comes with large Monte Carlo numerical uncertainties.

1. Introduction

In this note, we describe the validation of the implementation, in the MadAnalysis 5 framework [1–4], of the ATLAS-SUSY-2018-04 search [5] for direct stau production in events featuring two hadronic tau leptons and a large amount of missing transverse energy (E_T^{miss}). This analysis focuses on LHC proton-proton collisions at a center-of-mass energy of 13 TeV, and considers an integrated luminosity of 139fb^{-1}. The typical supersymmetric signal which this analysis is dedicated to is illustrated by the representative Feynman diagram shown in Fig. 1.

For the validation of our re-implementation, we have focused on a simplified model in which only a few electroweakly-interacting superpartners are relevant. The lightest neutralino ($\tilde{\chi}_1^0$) is taken as the lightest supersymmetric particle (LSP).

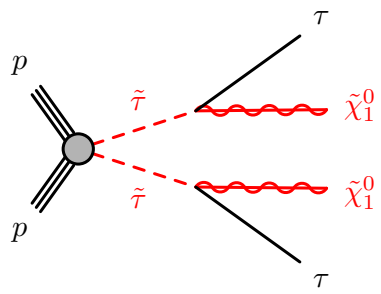

Fig. 1. The Feynman diagram for the process $pp \to \tilde{\tau}\tilde{\tau} \to \tilde{\chi}_1^0\tilde{\chi}_1^0\tau\tau$.

The stau-left ($\tilde{\tau}_L$) and stau-right ($\tilde{\tau}_R$) sleptons are moreover assumed to be mass degenerate and they do not mix. Therefore the gauge eigenstates ($\tilde{\tau}_L$,$\tilde{\tau}_R$) coincide with the mass eigenstates ($\tilde{\tau}_1$,$\tilde{\tau}_2$) in this theoretical framework. Furthermore, in order to suppress any other decay modes of the tau sleptons, the masses of all charginos and neutralinos are set to 2.5 TeV except for the $\tilde{\chi}_1^0$ neutralino. Hence, the single kinematically allowed decay mode of the staus is

$$\tilde{\tau} \to \tilde{\chi}_1^0\tau \tag{1}$$

Finally, all squarks, that do not contribute at leading-order, are decoupled as well.

This note is organized as follows. In Sec. 2, we present an outline of the analysis under consideration. It in particular includes definitions for the physics objects and event selections that we have implemented for our recasting exercise. Sec. 3 is dedicated to event generation in the context of the two considered benchmark for the validation or our re-implementation, and includes a comparison with official ATLAS results. In Sec. 4, we summarize our work.

2. Description of the analysis

This analysis targets a final state containing two hadronic tau leptons with a certain amount of missing transverse energy. The kinematics of the di-$\tau + E_T^{miss}$ system is used to reduce the contributions from Standard Model backgrounds. In Sec. 2.1, we first detail how the objects relevant for the analysis are reconstructed and defined. Then, in Sec. 2.2, we discuss the sequence of event selections that are applied in the aim of unravelling the signal from the background.

2.1. *Object definitions*

Jets are reconstructed by means of the anti-k_t algorithm [6] with a radius parameter set to $R = 0.4$. This analysis focuses on jets whose transverse momentum p_T^j and pseudorapidity η^j fulfill

$$p_T^j > 20 \text{ GeV} \quad \text{and} \quad |\eta^j| < 2.8. \tag{2}$$

Moreover, the selected jets that are tagged as originating from the fragmentation of a b-quark must satisfy the stronger requirements

$$p_T^b > 20 \text{ GeV} \quad \text{and} \quad |\eta^b| < 2.5. \tag{3}$$

In the considered analysis, a b-tagging working point with an average efficiency of 77% is used. This working point corresponds to c-jet and light-jet rejection rates of 4.9 and 110, respectively.

Electron candidates are required to have a transverse momentum p_T^e and pseudorapidity η^e obeying

$$p_T^e > 17 \text{ GeV} \quad \text{and} \quad |\eta^e| < 2.47. \tag{4}$$

Furthermore, all electron candidates are required to have both track and calorimeter isolations. The condition of the track isolation is

$$\sum p_{T,\text{tracks}}/p_T^e < 0.15 \quad \text{with} \quad \Delta R = \min(10 \text{ GeV}/p_T^e, 0.2), \tag{5}$$

the condition of the calorimeter isolation is

$$\sum E_{T,\text{calorimeter}}/p_T^e < 0.2 \quad \text{with} \quad \Delta R = 0.2, \tag{6}$$

and for high transverse momentum electron, we use instead of the two above conditions

$$\sum E_{T,\text{calorimeter}} < \max(0.015 \times p_T^e, 3.5 \text{ GeV}) \quad \text{with} \quad \Delta R = 0.2 \quad \text{if} \quad p_T^e > 200 \text{ GeV}. \tag{7}$$

Muon candidate definition is similar, although with slightly looser thresholds,

$$p_T^\mu > 14 \text{ GeV} \quad \text{and} \quad |\eta^\mu| < 2.7, \tag{8}$$

The condition of the track isolation is

$$\sum p_{T,\text{tracks}}/p_T^\mu < 0.15 \quad \text{with} \quad \Delta R = \min(10 \text{ GeV}/p_T^\mu, 0.3), \tag{9}$$

and the condition of the calorimeter isolation is

$$\sum E_{T,\text{tracks}}/p_T^\mu < 0.3 \quad \text{with} \quad \Delta R = 0.2. \tag{10}$$

In the ATLAS experiment, hadronically decaying tau lepton (τ_{had}) candidates are reconstructed with one or three associated charged pion tracks (prongs). For 1-prong (3-prong) τ lepton candidates, the signal efficiencies are 75% and 60% for the *medium* working point respectively. In the recasting based on MadAnalysis 5 that we implement in this work, the simulation of the detector response is performed with the Delphes 3 [7] software. We consider a tau-tagging efficiency of 100% with a misidentification probability of 0% at the level of Delphes 3, and handle medium and tight tau-tagging efficiencies through event reweighting factors extracted from the official ATLAS cutflow tables. Those factors are evaluated and included at the level of the analysis. Further details are given in Sec. 2.2.

Baseline tau lepton candidates are required to have

$$p_T^\tau > 50 \text{ (40) GeV} \quad \text{and} \quad |\eta^\tau| < 2.5 \tag{11}$$

for the leading (subleading) candidates, and the transition region between the barrel and endcap calorimeters ($1.37 < |\eta^\tau| < 1.52$) is excluded.

The object definition ends with some overlap removal conditions. The latter are implemented consistently to the analysis code provided through HEPData [8]. Tau leptons are removed if they are too close to an electron or a muon, with $\Delta R(\tau, e/\mu) < 0.2$. Electrons are then removed if they are too close to a muon, with $\Delta R(e, \mu) < 0.01$. Next, the jet collection is cleaned from those jets lying at an angular distance $\Delta R(j, e/\mu) < 0.2$ of a muon or an electron, and the electrons and muons that are too close to any of the remaining jets are removed if $\Delta R(e/\mu, j) < 0.4$. Finally, jets are removed if they are too close to one of the tau lepton candidates, with $\Delta R(j, \tau) < 0.2$.

2.2. *Event selection*

Because DELPHES 3 utilizes simplified and parameterized approaches to simulate different elements of the detector response, it is hard to emulate some of the properties relevant for the ATLAS-SUSY-2018-04 analysis, and therefore implement certain cut steps precisely. As a consequence, we have modelled several selections through event reweighting. This concerns first the trigger efficiency. Next, several reweighting factors are included to model specific features of the tau-tagging-based selections. This allows us to define the so-called *medium* and *tight* tau lepton cuts in our implementation, from an ideal detector parameterization in DELPHES 3.

After the object definitions introduced in the previous subsection, events with exactly two baseline tau leptons are selected. All events are required to pass either an *asymmetric di-*τ trigger for the low stau mass region (SR-lowMass) or a combined *di-*$\tau + E_T^{miss}$ ($E_T^{miss} > 150$ GeV) trigger for the high stau mass region (SR-highMass). This is coined *trigger and offline cuts* below. A trigger efficiency of 80% is applied in our recasting, after that we impose that the transverse momenta of the two leading tau candidates are larger than the offline p_T thresholds given in Table 1. In order to deal with the different tau candidate kinematic cuts that are applied in the 2015–2017 and 2018 data-taking periods, we randomly tag each event as originating from the 2015–2017 or 2018 data set. In practice, the probability of imposing the 2015–2017 (2018) data set thresholds is calculated from the ratio of the 2015–2017 (2018) integrated luminosity to the total luminosity of 139 fb^{-1}.

Moreover, we assume that the tau leptons which fired the triggers are those selected through the offline cuts. A trigger-level τ_{had} identification efficiency of 0.9 is correspondingly applied for each reconstructed tau lepton, which mimics the medium tau identification procedure for a tau lepton passing both online and offline requirements [9]. This leads to a total trigger reweighting factor of 64.8% that includes a global trigger efficiency of 80% and individual tau reconstruction efficiencies of 90%.

After the handling of the triggers described above, events with exactly two *medium* tau lepton candidates with opposite-sign (OS) electric charges are selected.

Table 1. Offline p_T thresholds for the leading (subleading) tau lepton candidate, in the case of the *asymmetric di-*τ (second column) and *di-*$\tau + E_T^{miss}$ (third column) triggers. This corresponds to a ditau efficiencies of about 80%.

Year	*asymmetric di-*τ	*di-*$\tau + E_T^{miss}$
2015-2017	95 (60) GeV	50 (40) GeV
2018	95 (75) GeV	75 (40) GeV

To treat the efficiency of selecting two offline mediumly tagged OS taus on top of a *di-tau(+*E_T^{miss}*)* trigger selection (as Delphes does not simulate charge misidentification), an additional event reweighting factor of 0.7 is enforced. This number is evaluated from the average ratio of the cut efficiencies provided by the ATLAS collaboration and those predicted by MadAnalysis 5 when the identification of two medium taus is not included at the cutflow step called *2 medium* τ *(OS) and 3rd medium* τ *veto* below.

In the next selection steps, a b-jet veto is enforced to reject events originating from top quark processes. Also, events featuring any additional light leptons (muons or electrons) are rejected. Finally, selection cuts common to both signal regions also include constraints on the reconstructed invariant mass of the two leading tau lepton system, $m(\tau_1, \tau_2)$. The latter is required to be larger than 120 GeV, in order to remove events exhibiting a pair of tau leptons stemming from low-mass resonances, Z boson, and Higgs boson decays (Z/H veto).

In the SR-lowMass region, a missing energy constraint of 75 GeV $< E_T^{miss} <$ 150 GeV is imposed to increase the signal sensitivity. Moreover, the two selected tau leptons are required to be tight tagged. The selection efficiency p_{tight} associated with two *medium* taus passing the *tight* working point requirements is extracted from the official ATLAS cutflow tables. We rely on the ratio of the number of surviving weighted events before applying the tight tau lepton requirement, and after applying it. We use $p_{tight} \simeq 0.70$.

In the SR-highMass region, the tight tagging efficiency is extracted similarly, with the exception that at least one of two tau leptons should pass the tight selection requirements and not both of them). We use here $p_{tight} + 2\sqrt{p_{tight}}(1 - \sqrt{p_{tight}}) \simeq 0.91$.

The *stransverse mass* m_{T2} variable [10, 11] is defined as

$$m_{T2} = min_{\mathbf{q}_T} \left[max(m_{T,\tau_1}(\mathbf{p}_{T,\tau_1}, \mathbf{q}_T), m_{T,\tau_2}(\mathbf{p}_{T,\tau_2}, \mathbf{p}_T^{miss} - \mathbf{q}_T)) \right], \qquad (12)$$

where $\mathbf{p}_{T,\tau_1}$ and $\mathbf{p}_{T,\tau_2}$ are the transverse momenta of the two tau lepton candidates. The transverse momentum vector of one of the invisible particle, $\mathbf{q}_T$, is chosen to minimize the larger of the two transverse mass m_{T,τ_1} and m_{T,τ_2}. The transverse mass m_T is defined by

$$m_T(\mathbf{p}_T, \mathbf{q}_T) = \sqrt{2(p_T q_T - \mathbf{p}_T \cdot \mathbf{q}_T)}. \qquad (13)$$

In MadAnalysis 5, the m_{T2} calculation can be done automatically through the function `PHYSICS->Transverse->MT2(vec1,vec2,ETmiss,Minvisible)`. In this expression, `vec1` and `vec2` stand for the two visible momenta, `ETmiss` for the missing transverse momentum and `Minvisible` for a test mass that should map the expected mass of the invisible state.

A lower bound on the m_{T2} variable of 70 GeV is imposed, in order to reduce the contamination from $t\bar{t}$ and WW events. Finally, the two tau lepton candidates are required to be well separated in the transverse plane, by $\Delta R(\tau_1, \tau_2) < 3.2$ and $|\Delta\phi(\tau_1, \tau_2)| > 0.8$ to further suppress the contributions of the Standard Model backgrounds.

3. Validation

3.1. *Event generation*

In order to validate our analysis, we rely on the MSSM implementation [12] available in the Feynrules [13] model database and shipped with thew MadGraph5_aMC@NLO event generator [14] as a UFO library [15].

We consider two benchmark points with masses $m(\tilde{\tau}, \tilde{\chi}_1^0) = (120, 1)$ GeV and $(280, 1)$ GeV to illustrate the validation of our re-implementation, as those correspond two scenarios for which official ATLAS cutflows and differential distributions are provided. The stau mixing matrix is additionally set to a unity matrix, so that the stau mass-eigenstates correspond to the right-handed and left-handed stau flavor-eigenstates.

We make use of MadGraph5_aMC@NLO version 2.6.7 [14] for hard-scattering event generation for each of the two stau eigenstates, in which we convolute leading-order matrix elements with the NNPDF23LO [16] set of parton distribution function. Our signal matrix elements include the potential emission of up to two additional partons, and the different contributions are merged according to the MLM scheme [17, 18]. We use a merging scale defined through the hard-scattering level parameter of MadGraph5_aMC2NLO `xqcut` $= m_{\tilde{\tau}}/4$.

The Pythia package version 8.244 [19] with the so-called $A14$ tune [20] has been used for the simulation of parton showering and hadronization. The simulation of the detector response has been performed by using Delphes 3.4.2 [7], that relies on FastJet [21] for object reconstruction.

We have tuned the ATLAS detector parameterization in Delphes 3 appropriately, according to the needs of the analysis. For example, loosened isolation criteria are applied so that isolation could be implemented fully at the analysis level. Moreover, the radius parameter and minimum transverse momentum used for jet reconstruction are reduced to 0.4 and 15 GeV respectively, and we have updated the b-tagging and tau-tagging performance. Finally, the `UniqueObjectFinder` module has been disabled as object overlap removal has been implemented at the level of the analysis.

Table 2. Cut-flow associated with a simplified model benchmark scenario defined by $m(\tilde{\tau}, \tilde{\chi}_1^0) = (120, 1)$ GeV and for the $pp \to \tilde{\tau}\tilde{\tau}$ production process. We compare ATLAS official results and MadAnalysis 5 predictions through the expected number of events after each cut and the corresponding efficiencies, and indicate their difference δ.

$\tilde{\tau}\tilde{\tau}$ **production with** $m(\tilde{\tau}, \tilde{\chi}_1^0) = (120, 1)$ **GeV**					
	ATLAS ($N_{weighted}$)	ϵ_i(%)	MA5 ($N_{weighted}$)	ϵ_i(%)	diff.(%)
Baseline cut	1686.80	-	1686.80	-	-
SR-low Mass					
Trigger and offline cuts	390.46	23.15	410.01	24.31	5.01
2 medium τ (OS) and 3rd medium τ veto	256.01	65.57	269.37	65.70	0.20
b-jet veto	250.59	97.88	263.66	97.88	-0.00
Light lepton veto	250.12	99.81	263.66	100	0.19
Z/H-veto	248.93	99.52	262.14	99.42	-0.10
$75 < E_T^{miss} < 150$ GeV	85.70	34.43	89.90	34.30	-0.38
2 tight τ	60.19	70.23	62.93	70.00	-0.33
$\lvert\Delta\phi(\tau,\tau)\rvert > 0.8$	60.14	99.92	62.75	99.72	-0.20
$\lvert\Delta R(\tau,\tau)\rvert < 3.2$	54.73	91.00	57.10	90.99	-0.01
$m_{T2} > 70$ GeV	9.78	17.87	14.65	25.66	43.58
All	-	0.58	-	0.87	49.80
SR-high Mass					
Trigger and offline cuts	101.23	6.00	96.35	5.71	-4.82
2 medium τ (OS) and 3rd medium τ veto	67.04	66.23	63.23	65.62	-0.91
b-jet veto	63.98	95.44	60.37	95.47	0.04
Light lepton veto	63.87	99.83	60.36	99.99	0.16
Z/H-veto	58.33	91.33	55.70	92.28	1.04
≥ 1 tight τ	57.29	98.22	50.69	91.00	-7.35
$\lvert\Delta\phi(\tau,\tau)\rvert > 0.8$	56.71	98.99	49.99	98.63	-0.36
$\lvert\Delta R(\tau,\tau)\rvert < 3.2$	51.74	91.24	45.41	90.84	-0.43
$m_{T2} > 70$ GeV	7.18	13.88	8.24	18.14	30.75
All	-	0.43	-	0.49	14.76

3.2. *Comparison with the official results*

In Tables 2 and 3, we compare predictions obtained with our implementation to the official results provided in the form of auxiliary tables by the ATLAS collaboration, for the two considered benchmark points with masses $m(\tilde{\tau}, \tilde{\chi}_1^0) = (120, 1)$ and $(280, 1)$ GeV respectively. For each cut, we have calculated the related efficiency

$$\epsilon_i = \frac{n_i}{n_{i-1}} \tag{14}$$

where n_i and n_{i-1} correspond to the number of events after and before the considered cut respectively. In our comparison, we have normalized the number of events

Table 3. Same as in Table 2 but for a scenario with supersymmetric masses $m(\tilde{\tau}, \tilde{\chi}_1^0) = (280, 1)$ GeV.

$\tilde{\tau}\tilde{\tau}$ **production with** $m(\tilde{\tau}, \tilde{\chi}_1^0) = (280, 1)$ **GeV**					
	ATLAS ($N_{weighted}$)	ϵ_i(%)	MA5 ($N_{weighted}$)	ϵ_i(%)	diff.(%)
Baseline cut	184.36	-	184.36	-	-
SR-low Mass					
Trigger and offline cuts	73.74	40.00	69.97	37.95	-5.12
2 medium τ (OS) and 3rd medium τ veto	47.86	64.90	46.23	66.08	1.81
b-jet veto	46.63	97.43	44.94	97.20	-0.24
Light lepton veto	46.49	99.70	44.94	99.99	0.30
Z/H-veto	44.84	96.45	43.83	97.54	1.13
$75 < E_T^{miss} < 150$ GeV	17.48	38.98	16.26	37.10	-4.83
2 tight τ	12.04	68.88	11.38	70.00	1.63
$\lvert\Delta\phi(\tau,\tau)\rvert > 0.8$	12.04	100	11.33	99.55	-0.45
$\lvert\Delta R(\tau,\tau)\rvert < 3.2$	11.08	92.03	10.35	91.32	-0.77
$m_{T2} > 70$ GeV	6.08	54.87	5.64	54.50	-0.68
All	-	3.30	-	3.06	-7.24
SR-high Mass					
Trigger and offline cuts	47.64	25.84	42.10	22.83	-11.64
2 medium τ (OS) and 3rd medium τ veto	30.72	64.48	27.80	66.03	2.40
b-jet veto	29.34	95.51	26.83	96.52	1.06
Light lepton veto	29.27	99.76	26.83	99.99	0.23
Z/H-veto	24.88	85.00	24.01	89.50	5.30
≥ 1 tight τ	24.21	97.31	21.85	91.00	-6.48
$\lvert\Delta\phi(\tau,\tau)\rvert > 0.8$	23.29	96.20	21.19	96.96	0.79
$\lvert\Delta R(\tau,\tau)\rvert < 3.2$	21.95	94.25	19.68	92.91	-1.42
$m_{T2} > 70$ GeV	14.35	65.38	13.37	67.91	3.88
All	-	7.78	-	7.25	-6.84

surviving the baseline cut n_0 as in the ATLAS cutflow. On the other hand, we have also evaluated the differences between the MadAnalysis 5 (ϵ_i(MA5)) and ATLAS (ϵ_i(ATLAS)) cut efficiencies through the quantity

$$\delta_i = \frac{\epsilon_i(\text{MA5}) - \epsilon_i(\text{ATLAS})}{\epsilon_i(\text{ATLAS})}. \tag{15}$$

We observe that for both scenarios, a good agreement is obtained at each step of the cutflow, with the exception of the last cut on the M_{T2} variable. For the $m(\tilde{\tau}, \tilde{\chi}_1^0) = (120, 1)$ GeV scenario, we hence obtain a disagreement of 30%–40% for both signal regions. In constrast, for the $m(\tilde{\tau}, \tilde{\chi}_1^0) = (280, 1)$ GeV scenario does not feature any strong issue at all, the two cutflow agreeing at the level of a few percent.

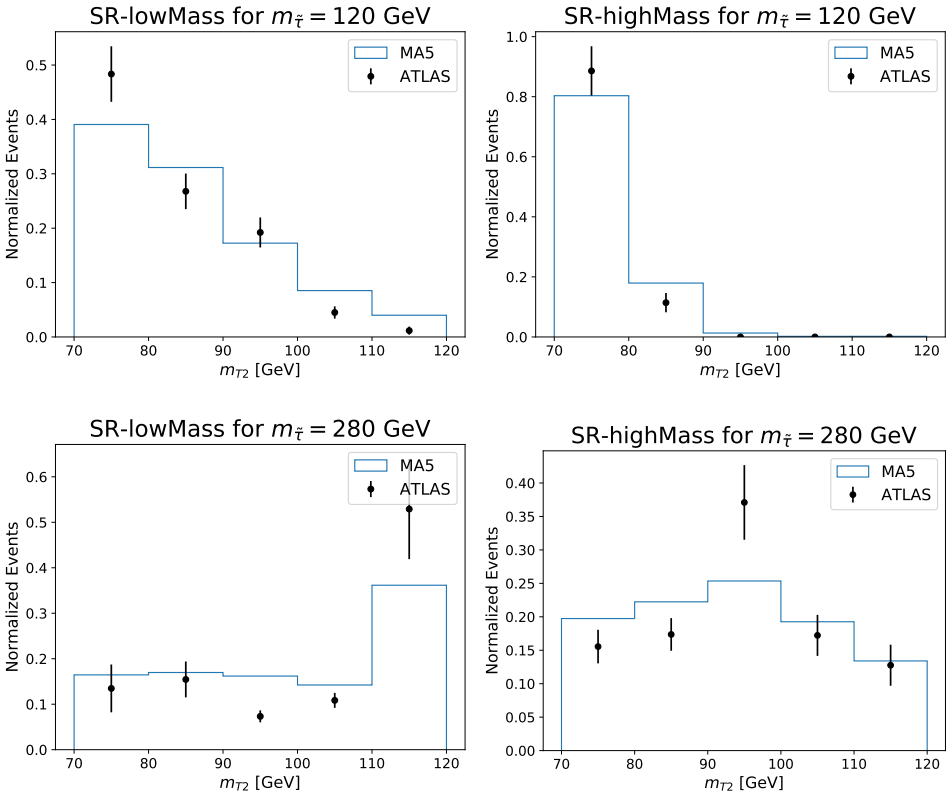

Fig. 2. The m_{T2} distributions after all cuts, for the SR-low Mass (left) and SR-high Mass (right) signal regions, and for the $m(\tilde{\tau}, \tilde{\chi}_1^0) = (120, 1)$ GeV (top panel) and $m(\tilde{\tau}, \tilde{\chi}_1^0) = (280, 1)$ GeV (bottom panel) scenarios.

By lack of additional publicly available experimental information, we have not been able to investigate this issue at a very deep level. We have nevertheless compared M_{T2} distributions as predicted by MadAnalysis 5 after all cuts, to those released by the ATLAS collaboration [8]. We have considered the two signal regions and both scenarios. Our results are shown in Fig. 2.

We observe that the global shape of the distribution is generally well reproduced, although the curves exhibit large differences that explain our findings at the level of the cutflow tables. However, one must note that the differences concern cases where a not so large number of (unweighted) events survive. Large Monte Carlo uncertainties of 10%–20% of percent are thus expected, both for our predictions and the ATLAS results.

To examine the impact of those yield differences on limit setting, we peformed a set of statistical analyses for various points in the stau and neutralino mass parameter space. The yields are normalized to NLO+NLL prediction [22, 23], and limits are calculated using the CL_s method [24]. The mass point is determined to

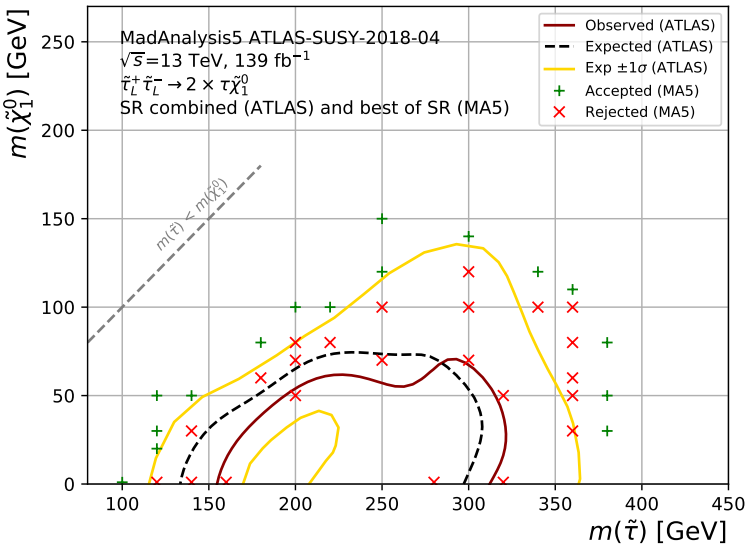

Fig. 3. Comparison of MadAnalysis 5 and official 95% CL exclusion contours. The point marked with red cross is excluded if one of signal region is rejected at $1 - \mathrm{CL}_s > 0.95$.

be excluded conservatively if one of the two signal regions leads to a 1-CL_s value greater than 0.95. This contrasts with the interpretations provided in the ATLAS publication [5], that rely on the combination of both signal regions. The results obtained with MadAnalysis 5 are presented in Fig. 3, along with the official ATLAS results.

The reproduced and official results agree generally well within 1σ. This suggests that the discrepancies related to the M_{T2} spectrum and the corresponding cut efficiency only affect the limits mildly. This is expected to be improved after combining the SR-lowMass and SR-highMass regions, as shown in the SModelS study of Ref. [25] that demonstrated that limits calculated from a single signal region of the considered analysis are overly enthusiastic.

Consequently, we consider our re-implementation as validated.

4. Conclusions

In this note, we detail our implementation of the ATLAS-SUSY-2018-04 search in the MadAnalysis 5 framework. Our analysis has been validated in the context of a supersymmetry-inspired simplified benchmark model in which the Standard Model is extended by a neutralino and a stau. Both stau chiralities are considered, as the stau is considered to decay into a tau lepton and a neutralino. Our validation relies on two different benchmark points in the parameter space.

By comparing our predictions for different cutflows for the two benchmarks with the official ones provided by the ATLAS collaboration in Ref. [5], we have found an

agreement at each step of the analysis, except for the last cut on the stranverse mass variable m_{T2} cut for the light stau scenario. While the shape of the distribution is correctly reproduced, large difference leads to a quite different cut efficiency. Due to the lack of more information, we have however not been able to investigate the issue more precisely. By further comparing exclusion contours obtained with MadAnalysis 5 to those provided by the ATLAS collaboration, we however observe that this only impacts the limits at the level of 1σ. As a consequence, we have considered our re-implementation as validated.

The MadAnalysis 5 C++ code is available from the MadAnalysis 5 dataverse (https://doi.org/10.14428/DVN/UN3NND) [26]. The material relevant for the validation benchmarks has been obtained from HEPData [8].

References

1. E. Conte and B. Fuks, *Int. J. Mod. Phys. A* **33**, 1830027 (2018), arXiv:1808.00480 [hep-ph].
2. B. Dumont, B. Fuks, S. Kraml, S. Bein, G. Chalons, E. Conte, S. Kulkarni, D. Sengupta and C. Wymant, *Eur. Phys. J. C* **75**, 56 (2015), arXiv:1407.3278 [hep-ph].
3. E. Conte, B. Dumont, B. Fuks and C. Wymant, *Eur. Phys. J. C* **74**, 3103 (2014), arXiv:1405.3982 [hep-ph].
4. E. Conte, B. Fuks and G. Serret, *Comput. Phys. Commun.* **184**, 222 (2013), arXiv:1206.1599 [hep-ph].
5. ATLAS Collaboration, G. Aad *et al.*, *Phys. Rev. D* **101**, 032009 (2020), arXiv:1911.06660 [hep-ex].
6. M. Cacciari, G. P. Salam and G. Soyez, *JHEP* **04**, 063 (2008), arXiv:0802.1189 [hep-ph].
7. DELPHES 3 Collaboration, J. de Favereau, C. Delaere, P. Demin, A. Giammanco, V. Lemaître, A. Mertens and M. Selvaggi, *JHEP* **02**, 057 (2014), arXiv:1307.6346 [hep-ex].
8. ATLAS Collaboration, *10.17182/hepdata.92006.v2* (2020).
9. ATLAS Collaboration, *ATLAS-CONF-2017-029* (5 2017).
10. C. Lester and D. Summers, *Phys. Lett. B* **463**, 99 (1999), arXiv:hep-ph/9906349.
11. H.-C. Cheng and Z. Han, *JHEP* **12**, 063 (2008), arXiv:0810.5178 [hep-ph].
12. C. Duhr and B. Fuks, *Comput. Phys. Commun.* **182**, 2404 (2011), arXiv:1102.4191 [hep-ph].
13. A. Alloul, N. D. Christensen, C. Degrande, C. Duhr and B. Fuks, *Comput. Phys. Commun.* **185**, 2250 (2014), arXiv:1310.1921 [hep-ph].
14. J. Alwall, R. Frederix, S. Frixione, V. Hirschi, F. Maltoni, O. Mattelaer, H. S. Shao, T. Stelzer, P. Torrielli and M. Zaro, *JHEP* **07**, 079 (2014), arXiv:1405.0301 [hep-ph].
15. C. Degrande, C. Duhr, B. Fuks, D. Grellscheid, O. Mattelaer and T. Reiter, *Comput. Phys. Commun.* **183**, 1201 (2012), arXiv:1108.2040 [hep-ph].
16. R. D. Ball *et al.*, *Nucl. Phys. B* **867**, 244 (2013), arXiv:1207.1303 [hep-ph].
17. M. L. Mangano, M. Moretti, F. Piccinini and M. Treccani, *JHEP* **01**, 013 (2007), arXiv:hep-ph/0611129.
18. J. Alwall, S. de Visscher and F. Maltoni, *JHEP* **02**, 017 (2009), arXiv:0810.5350 [hep-ph].
19. T. Sjöstrand, S. Ask, J. R. Christiansen, R. Corke, N. Desai, P. Ilten, S. Mrenna,

S. Prestel, C. O. Rasmussen and P. Z. Skands, *Comput. Phys. Commun.* **191**, 159 (2015), arXiv:1410.3012 [hep-ph].
20. (11 2014).
21. M. Cacciari, G. P. Salam and G. Soyez, *Eur. Phys. J. C* **72**, 1896 (2012), arXiv:1111.6097 [hep-ph].
22. B. Fuks, M. Klasen, D. R. Lamprea and M. Rothering, *Eur. Phys. J. C* **73**, 2480 (2013), arXiv:1304.0790 [hep-ph].
23. B. Fuks, M. Klasen, D. R. Lamprea and M. Rothering, *JHEP* **01**, 168 (2014), arXiv:1310.2621 [hep-ph].
24. A. L. Read, *J. Phys.* **G28**, 2693 (2002), [,11(2002)].
25. C. K. Khosa, S. Kraml, A. Lessa, P. Neuhuber and W. Waltenberger, *LHEP* **158**, 2020 (5 2020), arXiv:2005.00555 [hep-ph].
26. J. Lim, C.-T. Lu, J.-H. Park and J. Park, *10.14428/DVN/UN3NND* (2020).